

Date of current version September 18, 2022.

Digital Object Identifier 10.1109/ACCESS.2022.DOI

# Machine Learning Based Transient Stability Emulation and Dynamic System Equivalencing of Large-Scale AC-DC Grids for Faster-Than-Real-Time Digital Twin

SHIQI CAO<sup>1</sup>, (Student Member, IEEE), VENKATA DINAVAH<sup>2</sup>, (Fellow, IEEE), AND NING LIN,<sup>3</sup> (Member, IEEE)

<sup>1</sup>Electrical and Computer Engineering Department, University of Alberta, Edmonton, AB T6G 2R3 CA (e-mail: sc5@ualberta.ca)

<sup>2</sup>Electrical and Computer Engineering Department, University of Alberta, Edmonton, AB T6G 2R3 CA (e-mail: dinavahi@ualberta.ca)

<sup>3</sup>Powertech Labs Inc, Surrey, BC V3W 7R7 CA (e-mail: ning3@ualberta.ca)

Corresponding author: Shiqi Cao (e-mail: sc5@ualberta.ca).

This work is supported by the Natural Science and Engineering Research Council of Canada (NSERC).

**ABSTRACT** Modern power systems have been expanding significantly including the integration of high voltage direct current (HVDC) systems, bringing a tremendous computational challenge to transient stability simulation for dynamic security assessment (DSA). In this work, a practical method for energy control center with the machine learning (ML) based synchronous generator model (SGM) and dynamic equivalent model (DEM) is proposed to reduce the computational burden of the traditional transient stability (TS) simulation. The proposed ML-based models are deployed on the field programmable gate arrays (FPGAs) for faster-than-real-time (FTRT) digital twin hardware emulation of the real power system. The Gated Recurrent Unit (GRU) algorithm is adopted to train the SGM and DEM, where the training and testing datasets are obtained from the off-line simulation tool DSATools<sup>TM</sup>/TSAT<sup>®</sup>. A test system containing 15 ACTIVSg 500-bus systems interconnected by a 15-terminal DC grid is established for validating the accuracy of the proposed FTRT digital twin emulation platform. Due to the complexity of emulating large-scale AC-DC grid, multiple FPGA boards are applied, and a proper interface strategy is also proposed for data synchronization. As a result, the efficacy of the hardware emulation is demonstrated by two case studies, where an FTRT ratio of more than 684 is achieved by applying the GRU-SGM, while it reaches over 208 times for hybrid computational-ML based digital twin of AC-DC grid.

**INDEX TERMS** AC-DC grid, digital twin, dynamic equivalents, faster-than-real-time, field programmable gate arrays, gated recurrent unit, machine learning, parallel processing, power system stability, real-time systems, recurrent neural networks, synchronous generator.

## I. INTRODUCTION

Transient stability (TS) simulation plays a paramount role in dynamic security assessment of power systems. With the increasing size and complexity of modern power systems, the TS simulation requires considerable computational effort [1]. The commonly used security indices for a large-scale transmission network are obtained from TS simulations, which provide critical data for analyzing the system stability such

as rotor angles, bus voltages, and frequencies. The current industry practice is able to accelerate the TS simulation in real-time execution due to the availability of the high-performance hardware [2]. However, the existing solutions for TS simulation are based on the numerical solutions of model equations that represent the dynamic process of the nonlinear system components.

In the last few decades, dynamic equivalencing has been

adopted for dealing with the large-scale systems for TS simulation, which divides the system into “study zone” where the dynamic phenomena occur and “external system” where the system part needs to be replaced [2]. The dynamic equivalent model is obtained by reducing the number of generator and the network nodes. Currently, the main approaches of dynamic equivalencing are largely classified into the following three directions: 1) Coherency methods [1], [3]–[5], which are achieved by replacing a coherent group of machines in the external system with an equivalent generator and attaching it to a common bus. 2) Modal methods [6]–[8], which focus on the less damped modes. The linear equivalents are obtained by applying reduction techniques that eliminate the high damped modes. Meanwhile, the modal methods are also cooperated with the coherency methods to identify the coherent groups [8]. 3) Estimation methods [10]–[13], which basically utilize measurements or simulation based results to estimate the parameters of the equivalent model.

Although valuable contributions have been made, the computational requirements are still heavy by the aforementioned approaches, such as the eigenvalue analysis, diagonalization of the modal approach, or identification of the coherency groups. In this work, machine learning (ML) based dynamic equivalent models are proposed for both synchronous generator and external networks for TS emulation. Artificial neural network (ANN) based power system dynamic equivalencing has been previously proposed in [14]; however, traditional ANN-based equivalent models are relatively simple, and cannot meet the requirements for long-term prediction for a large-scale network. Therefore, the Gated Recurrent Unit (GRU) algorithm is utilized, which is a variant of the Long Short-Term Memory (LSTM) network that has a higher accuracy in representing the non-linear parts for dynamic equivalencing [15].

Although compared with ANN-based algorithms, the GRU-based dynamic equivalent model requires more hardware resources and inferring time, these shortcomings can be effectively minimized by the FPGA. The reconfigurability of FPGAs enables each system component to be designed according to its function [16]. The proposed FTRT emulation can therefore operate as a digital twin of the real power system to predict its performance and provide remedial solutions after detection of a disturbance. Meanwhile, the sufficient hardware resources in the latest Xilinx Virtex<sup>®</sup> UltraScale+<sup>™</sup> series boards allow the entire AC-DC grid to be deployed on the platform after proper system partitioning and allocation. As a result, the hybrid computational-ML based digital twin of AC-DC grid can be executed 208 times faster than real-time mode.

The paper is expanded as follows: Section II introduces the background of TS simulation and the multi-mass shaft synchronous generator model. The detailed training procedures and validation of the proposed GRU-SGM is specified in Section II. Section III demonstrates GRU-DEM for a large-scale AC-DC grid and the interface strategy. The hardware design of the proposed algorithms on FPGA boards is given

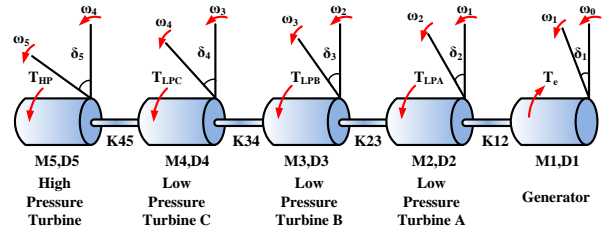


FIGURE 1. Five-mass torsional shaft system.

in Section VI. The FTRT emulation results and subsequent analysis are provided in Section V. Section VI presents the conclusion and the application of GRU-based equivalent models.

## II. PART I: MACHINE LEARNING BASED MODELING OF SYNCHRONOUS GENERATOR

### A. TRANSIENT STABILITY PROBLEM

TS simulation is essentially analyzing the rotor-angle, voltage, and frequency stability of synchronous generators. The dynamics of generators and their auxiliary controllers are represented by a set of nonlinear differential-algebraic equations (DAEs) given below:

$$\frac{d\mathbf{X}(t)}{dt} = F(\mathbf{X}(t), \mathbf{V}(t), \mathbf{u}(t)), \quad (1)$$

$$G(\mathbf{X}(t), \mathbf{V}(t)) = \mathbf{0}, \quad (2)$$

where  $\mathbf{X}$  is the vector of the state variables,  $\mathbf{V}$  refers to the bus voltage vector, and  $\mathbf{u}$  represents the vector of inputs from the generator controllers such as mechanical torque ( $T_m$ ). The initial conditions are provide in (3), which can be obtained by steady-state estimation.

$$\mathbf{X}_0 = \mathbf{X}(t_0). \quad (3)$$

### B. DETAILED SYNCHRONOUS GENERATOR COMPUTATIONAL MODEL

To achieve a high accuracy, a detailed 17<sup>th</sup>-order multi-mass synchronous machine model (SGM) is chosen as the training target for the ML-based SGM, which includes four electrical equations consisting two windings on  $d$ -axis and two damping windings on  $q$ -axis, and an excitation system with three DAEs. In addition, a five-mass shaft system composed of the four-mass-turbine shaft connecting with the generator rotating shaft is also applied for training the ML-based SGM, as shown in Fig. 1. The ten mechanical equations for the multi-mass torsional shaft model can be written as:

$$\frac{d\delta_1}{dt} = \omega_R \cdot \Delta\omega_1(t), \quad (4)$$

$$\frac{d\Delta\omega_1}{dt} = \frac{[K_{12}(\delta_2(t) - \delta_1(t)) - T_e(t) - D_1 \cdot \Delta\omega_1(t)]}{2H_1}, \quad (5)$$

$$\frac{d\delta_n}{dt} = \omega_R \cdot \Delta\omega_n(t), \quad (6)$$

$$\frac{d\Delta\omega_n}{dt} = \frac{1}{2H_n} [T_n(t) + K_n^{n+1}(\delta_{n+1}(t) - \delta_n(t) - K_n^n (\delta_n(t) - \delta_{n-1}(t)) - D_n \Delta\omega_n(t)], \quad (7)$$

$$\frac{d\delta_5}{dt} = \omega_R \cdot \Delta\omega_5(t), \quad (8)$$

$$\frac{d\Delta\omega_5}{dt} = \frac{[T_5(t) - K_{45}(\delta_5(t) - \delta_4(t)) - D_5 \Delta\omega_5(t)]}{2H_5}, \quad (9)$$

where the subscript  $n$  in (6) and (7) represents to *Mass* 2-4, and variables with subscript 1 constitute the mechanical functions of the generator shaft.  $T_5$ , and  $T_n$  are the mechanical torques of steam turbines, which are obtained from the governor system. The electrical equations describing the generator are given as

$$\frac{d\psi_{fd}}{dt} = \omega_R \cdot [e_{fd}(t) - R_{fd}i_{fd}(t)], \quad (10)$$

$$\frac{d\psi_{1d}}{dt} = -\omega_R \cdot R_{1d}i_{1d}(t), \quad (11)$$

$$\frac{d\psi_{1q}}{dt} = -\omega_R \cdot R_{1q}i_{1q}(t), \quad (12)$$

$$\frac{d\psi_{2q}}{dt} = -\omega_R \cdot R_{2q}i_{2q}(t), \quad (13)$$

The excitation system model is comprised of the power system stabilizer (PSS) and automatic voltage regulator (AVR), the corresponding equations are given below.

$$\frac{dv_1}{dt} = \frac{[v_t(t) - v_1(t)]}{T_R}, \quad (14)$$

$$\frac{dv_2}{dt} = K_{stab} \cdot \Delta\omega(t) - \frac{v_2(t)}{T_w}, \quad (15)$$

$$\frac{dv_3}{dt} = \frac{[T_1 \cdot dv_2/dt + v_2(t) - v_3(t)]}{T_2}. \quad (16)$$

where the time-varying variables in (4)-(13) contribute to vectors  $\mathbf{U}(t)$  and  $\mathbf{X}(t)$  in (2), and the remaining coefficients such as  $\omega_R$ ,  $H_{1-5}$ ,  $D_{1-5}$ ,  $R_{fd}$ ,  $R_{1d}$ ,  $R_{1q}$ ,  $R_{2q}$ ,  $T_R$ ,  $K_{stab}$ ,  $T_w$ ,  $T_1$ , and  $T_2$  are constant parameters of generators and the excitation system, which can be found in [17].

### C. MACHINE LEARNING STRATEGY

The commonly used machine learning strategies for modeling the components in modern power systems are discussed, including traditional artificial neural network (ANN) and recurrent neural network (RNN). Recently, a widespread ML method named convolutional neural network (CNN) has witnessed an increase in many applications. Compared with CNN, the RNN has better performance than CNN regarding ML modeling of time-series signals because of its effectiveness and long-term prediction ability. Even though many newer applications of transform in natural language processing (NLP) have emerged in recent years, considering the features of the power system, hardware resource consumption, and latency, it is more efficient to utilize RNN

TABLE 1. Comparison of various ML strategies

Features	ANN	CRNN	GRU	LSTM
Accuracy	★	★★	★★★	★★★★
Complexity	★	★★	★★★	★★★★
Resource Consumption	★★★★	★	★★	★★★
Long-Term Prediction	No	No	Yes	Yes

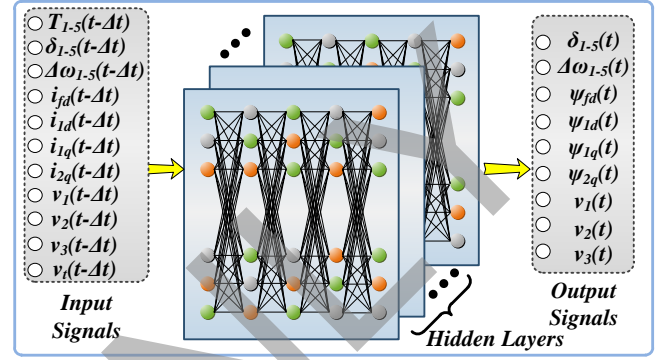


FIGURE 2. Lumped GRU model of synchronous generator.

with a more straightforward structure for ML modeling in this paper.

The complexity and accuracy of ANN [18], [19], convolutional recurrent neural network (CRNN) [20], GRU [21], and long short-term memory (LSTM) [22] for modeling power electronic devices are compared in the literature [24]. Meanwhile, the techniques mentioned above are compared in Table 1. ANN has the lowest accuracy and the most hardware resource consumption, which is not considered for hardware design. As for RNNs (CRNN, GRU, and LSTM), the more accurate it is, the more complex the structure and resource consumption it needs, resulting in a longer execution time. Although CRNN has acceptable accuracy and complexity for hardware emulation, the capability of long-term prediction makes it not suitable for transient stability simulation. GRU is a relatively low-resource-consumption RNN with reasonably high accuracy, which is more accurate than ANN and CRNN, close to LSTM, but the resource consumption is much smaller than LSTM. GRU is a substitute for LSTM with long-term predictive capability, which makes it suitable for time-series prediction (e.g., traffic flow prediction [23]). Since the forget gate and the input gate in LSTM are replaced by a single update gate in GRU, resulting in lower complexity for GRU. After a trade-off between accuracy and hardware resource consumption, the GRU is selected as the main training method for ML-based synchronous generator model and dynamic equivalent model. The working principles of the GRU method are given below:

1) Update process: the update matrix  $\mathbf{Z}$  is calculated by input  $\mathbf{X}$  and previous state  $\mathbf{H}^{t-1}$ , as given below:

$$\mathbf{Z} = \sigma(\mathbf{W}_z[\mathbf{X}, \mathbf{H}^{t-1}] + \mathbf{B}_z). \quad (17)$$

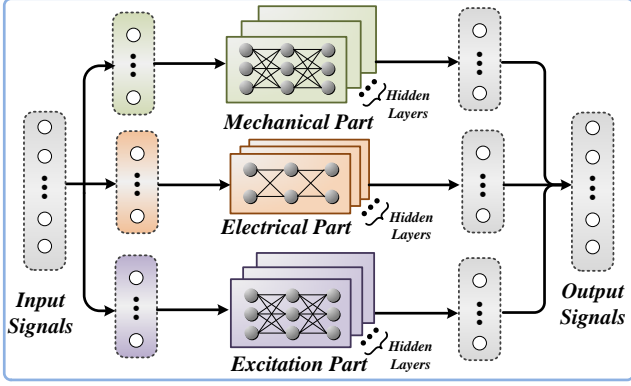


FIGURE 3. Partitioned GRU model of synchronous generator.

GRU is assisted by the update gate in determining how much information from the previous and the present time-step should be transmitted into current state. It is quite important since the GRU may choose to replicate all previous information to minimize the risk of disappearing gradients.

2) Reset process:

$$\mathbf{R} = \sigma(\mathbf{W}_r[\mathbf{X}, \mathbf{H}^{t-1}] + \mathbf{B}_r), \quad (18)$$

where the reset matrix  $\mathbf{R}$  is obtained from input  $\mathbf{X}$  and previous state  $\mathbf{H}^{t-1}$ . This matrix  $\mathbf{R}$  has the same equation as the update gate matrix  $\mathbf{Z}$ , but its parameters and applications are different. This gate is used to select how much of the past or current information to forget.

3) Current memory process:

$$\mathbf{H}_r^{t-1} = \mathbf{H}^{t-1} \mathbf{R}, \quad (19)$$

$$\mathbf{H}' = \tanh(\mathbf{W}_h[\mathbf{X}, \mathbf{H}_r^{t-1}] + \mathbf{B}). \quad (20)$$

The previously acquired reset gate processes the historical information  $\mathbf{H}^{t-1}$  to get  $\mathbf{H}_r^{t-1}$ , which determines the past information to be maintained and abandoned. Then, the current memory  $\mathbf{H}'$  is constructed by the processed historical information and the current input  $\mathbf{X}$ , as shown in (20) where the hyperbolic tangent activation function is used.

4) Final transfer memory process:

$$\mathbf{H}^t = \mathbf{Z} \mathbf{H}^{t-1} + (\mathbf{I} - \mathbf{Z}) \mathbf{H}'. \quad (21)$$

$\mathbf{H}^t$ , a vector that stores information from the current unit, is computed and passed on to the next unit. The update gate matrix  $\mathbf{Z}$ , which decides what information needs to be gathered in the current memory content  $\mathbf{H}'$  and the prior time step  $\mathbf{H}^{t-1}$ , must be used in this procedure.

A lumped GRU model with inputs and outputs is depicted in Fig. 2, which may be developed without specific expertise. According to (4)-(16), the input vector  $\mathbf{X}$  can be defined as:

$$\mathbf{X} = [T_{1-5}, \delta_{1-5}, \Delta\omega_{1-5}, i_{fd}, i_{1d}, i_{1q}, i_{2q}, v_1, v_2, v_3, v_t]^T. \quad (22)$$

Since the proposed GRU-SGM is conducted on the FPGA boards, the sequence length, hidden size, and layers that may

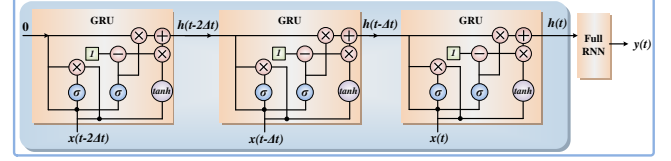


FIGURE 4. GRU structure for each part (mechanical, electrical, and excitation) of synchronous generator.

influence the hardware resource consumption should be properly defined. In this work, the lumped model is divided into three parts depending on machine operation knowledge, as illustrated in Fig. 3. As for the hyper-parameter optimization, we choose the model hyper-parameters based on experience. Then we train the model, evaluate its accuracy and start the process again. In the beginning, based on experience the hidden size ranges from 20 to 100, and the hidden layer is decided as 1 or 2 to reduce the hardware consumption. After modifying the hyperparameters during the training process, the layer number is one, hidden size is 30 and the sequence length is three for GRU-SGM. The structure of an unrolled GRU model is shown in Fig. 4.

The partitioned model enables the three portions to be calculated in parallel and thus lower the hide size, saving hardware resource usage and speeding up execution without compromising accuracy. And this division is based on expertise and has no bearing on accuracy. The GRU model of the mechanical part of the machine can be trained based on the input and output variables of (4)-(9). The GRU can then represent the current and flux linkage parts, in the same way as (10)-(13). In terms of excitation system, the effect of the third GRU model is similar to that of (14)-(16).

#### D. DATASETS AND TRAINING

Taking the IEEE 39-bus system for example, the training data is obtained from several three-phased to ground faults, as given in Fig. 5. As aforementioned, the ML-based model is trained to represent the 17<sup>th</sup>-order synchronous generator, which contains 5-mass torsional shaft and excitation system. Due to the various generation levels and control parameters, each generator should be trained independently. Three different faults are simulated in the offline simulation tool TSAT<sup>®</sup> to provide the dataset for training a single generator. Since the fault locations have significant impacts on the dynamics of generator state variables, the fault buses are chosen from closest to furthest, which are located at Bus 39, 15, and 29 for training the Gen 10. As a result, there are 30 three-phase-to-ground faults to be simulated in total to train the ten generators in the IEEE 39-bus system.

The training data set comprises data on both normal and abnormal operating circumstances since the system includes a fault state. The model's input and output contain substantial variations; therefore, a data set with a wide range of variations is highly essential for GRU model training. In practice, 1 ms is chosen as the time-step, and a 20-second dataset is captured, which means the dataset of each fault contains



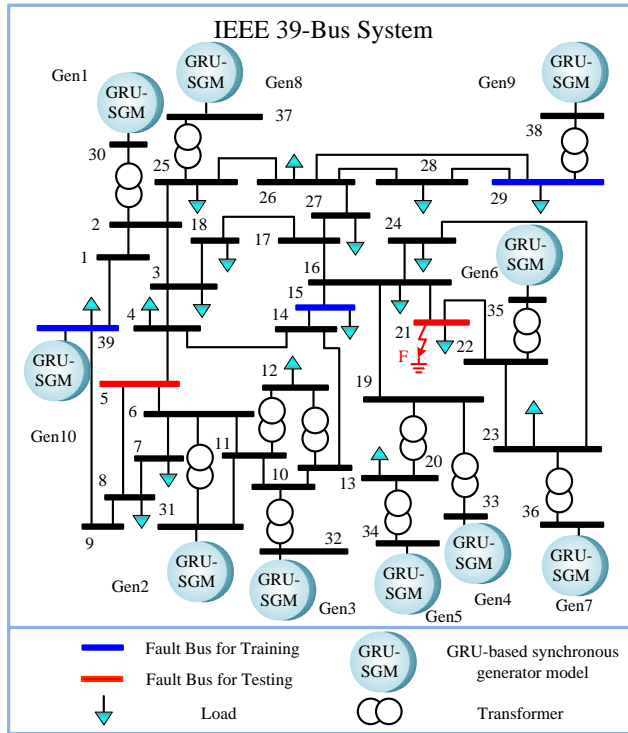


FIGURE 5. Topology of IEEE 39-bus system with ML-based synchronous generator models.

10,000 points. As a result, there are 30,000 points in total to train a single generator. 70% of it is utilized for training, while the remaining 30% is used for testing. For the training of the GRU model, it is not necessary to input all the training data obtained into the program, which will result in the training time being too long. After shuffling the training data, the data processing program samples the data set at regular intervals and sends it to the training program so that the obtained data set ensures generality and dramatically reduces the size. The same data set will send to the training program several times (epoch numbers) to obtain an accurate GRU-based model. Meanwhile, Adam algorithm [25] is chosen as an adaptive learning rate optimization method to minimize the errors during training processes.

The estimated offline simulation time for a three-phase-to-ground fault is ranging from 7-8 s based on our lab computer equipped with AMD® Ryzen 9 3950X CPU. Theoretically, the total time for obtaining the dataset of the generators is less than 240 s. Meanwhile, the TSAT® allows simulating several contingencies in sequence without time delay. The estimated time for Part I and Part II can be realized by uploading a file with contingency information to TSAT®. The proposed models are trained in a 196-node cluster after GRU parameter design, where each node contains two Intel® Silver 4216 Cascade Lake central processing units (CPUs). As mentioned, the lumped GRU model is divided into three parts, resulting in a partitioned GRU model. Since the inputs and outputs of each generator parts are independent, the three

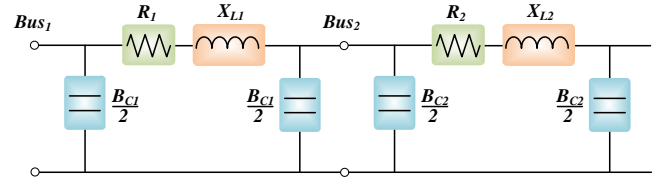


FIGURE 6. Transmission line  $\pi$  model.

parts of the partitioned GRU-SGM are trained in parallel to save the training time. Meanwhile, the training time for the mechanical part is a little bit long. To obtain a complete generator model, the electrical part and control system part should wait the mechanical part to finish, the total training time for the synchronous machine cost about 8 h training on a cluster node requiring within 10 GB memory. Then, the training results, weights and bias of the GRU models, are obtained and saved in Pytorch framework.

### E. HYBRID COMPUTATIONAL-ML SOLUTION SCHEME FOR TS SIMULATION

The network transients of TS simulation are typically calculated in the form of nodal equations. The main components in the AC network include transmission lines, compensators, and loads, which are represented by the admittance matrix solved at constant frequency. The transmission lines in TS simulation are modeled using a lumped  $\pi$  model, as given in the Fig. 6. R, X, and B refer to the resistance, reactance, and susceptance of the transmission line. The element  $Y(1, 2)$  in the admittance matrix can be calculated as:

$$Y(1, 2) = -\frac{1}{R_1 + jX_{L1}} = Y(2, 1), \quad (23)$$

$$Y(2, 2) = \frac{1}{R_1 + jX_{L1}} + \frac{1}{R_2 + jX_{L2}} + \frac{j(B_{C1} + B_{C2})}{2}. \quad (24)$$

Meanwhile, the fixed compensators and loads can be expressed as:

$$Y_{Load} = \frac{P_{Load} + j \cdot (Q_{Load})}{V_{Bus}^2}. \quad (25)$$

Then the network equation for TS simulation can be obtained as:

$$\begin{bmatrix} \mathbf{I}_m^{ML} \\ \mathbf{I}_r \end{bmatrix} = \begin{bmatrix} \mathbf{Y}_{mm} & \mathbf{Y}_{mr} \\ \mathbf{Y}_{rm} & \mathbf{Y}_{rr} \end{bmatrix} \begin{bmatrix} \mathbf{E}_m^{ML} \\ \mathbf{E}_r \end{bmatrix}, \quad (26)$$

where the subscript  $m$  refer to the generator nodes with current injection,  $r$  represents the remaining nodes without synchronous generators, the superscript  $ML$  denotes the variables that are calculated from GRU-SGM. Due to the absence of current injection in the non-generator buses, the current vector of the remaining nodes  $\mathbf{I}_r = [0]$  and  $\mathbf{I}_m^{ML}$  can be derived as

$$\mathbf{I}_m^{ML} = \mathbf{Y}_{reduced} \cdot \mathbf{E}_m^{ML}, \quad (27)$$

where  $\mathbf{Y}_{reduced}$  is expanded as  $\mathbf{Y}_{mm} - \mathbf{Y}_{mr} \mathbf{Y}_{rr}^{-1} \mathbf{Y}_{rm}$ . It is noticed that the generator voltages  $\mathbf{E}_m^{ML}$  are not directly

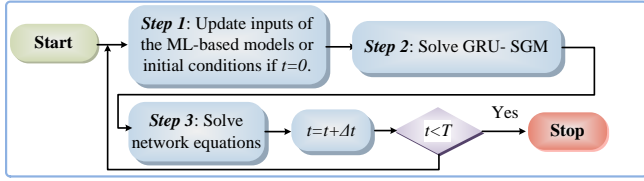


FIGURE 7. Procedure for the hybrid computational-ML based TS emulation.

TABLE 2. Relative errors of rotor angles under various systems

System	Gen.	25 Epoch	50 Epoch	75 Epoch	100 Epoch
IEEE 39-bus	10	11.43%	5.93%	1.36%	<b>0.65%</b>
IEEE 118-bus	54	16.13%	8.03%	1.50%	0.94%
ACTIVSg 500-bus	90	13.35%	6.69%	1.39%	0.84%

known, which are evaluated by the state variables after each step of integration. The relationship between generator voltages and currents can be expressed by the following equations.

$$E_D^{ML} = I_D^{ML} \cdot u_1 + I_Q^{ML} \cdot u_3 + u_5, \quad (28)$$

$$E_Q^{ML} = I_D^{ML} \cdot u_2 + I_Q^{ML} \cdot u_4 + u_6, \quad (29)$$

where  $u_{1-6}$  can be obtained by the acquirement of state variables, which are given in [17]. Thus, the emulation procedure for the hybrid computational-ML based AC-DC grid is illustrated in Fig. 7.

### F. INFERRING FROM THE TRAINED MODEL

As mentioned, some tests have been done in the training process. Although these GRU models are optimized and elevated by the test datasets, they should be further tested by the practical application operation. The trained GRU-SGM is tested on a standard IEEE 39-bus system containing ten generators and validated by the offline simulation tool TSAT®. The accuracy of the proposed model is related to the epoch of training. Fig. 8 (a)-(c) provides the rotor angles of Gen 10 of a three-phase-to-ground fault at Bus 5, and 21 lasting 150 ms of various epoch numbers. The representation of the three-phase fault in TS simulation is given in Fig. 9.  $V_a$  and  $I_a$  refer to the voltage and current of the ground loop. The equivalent fault impedance  $Z_{ef}$  is zero when a three-phase-to-ground fault occurs. The state variables  $\Delta\omega_1$ ,  $\psi_{fd}$ ,  $\psi_{1d}$ ,  $\psi_{1q}$ ,  $\psi_{2q}$ , and  $v_3$  are also illustrated in Fig. 8 (c)-(h). The zoomed-in plots in Fig. 8 indicate that with the epoch number increasing the higher accuracy can be obtained. Meanwhile, to further demonstrate the accuracy of GRU-SGM for TS emulation, the relative errors of rotor angles from various generators under different epoch numbers are given in Fig. 10. The accuracy of the proposed model is illustrated by the relative errors which are calculated by the following formula:

$$\epsilon = \frac{|\delta_{GRU} - \delta_{TSAT}|}{\delta_{TSAT}} \times 100\%. \quad (30)$$

Fig. 10 and zoomed-in plots in Fig. 8 (a), (d), and (h) indicate that with the epoch number increasing the higher

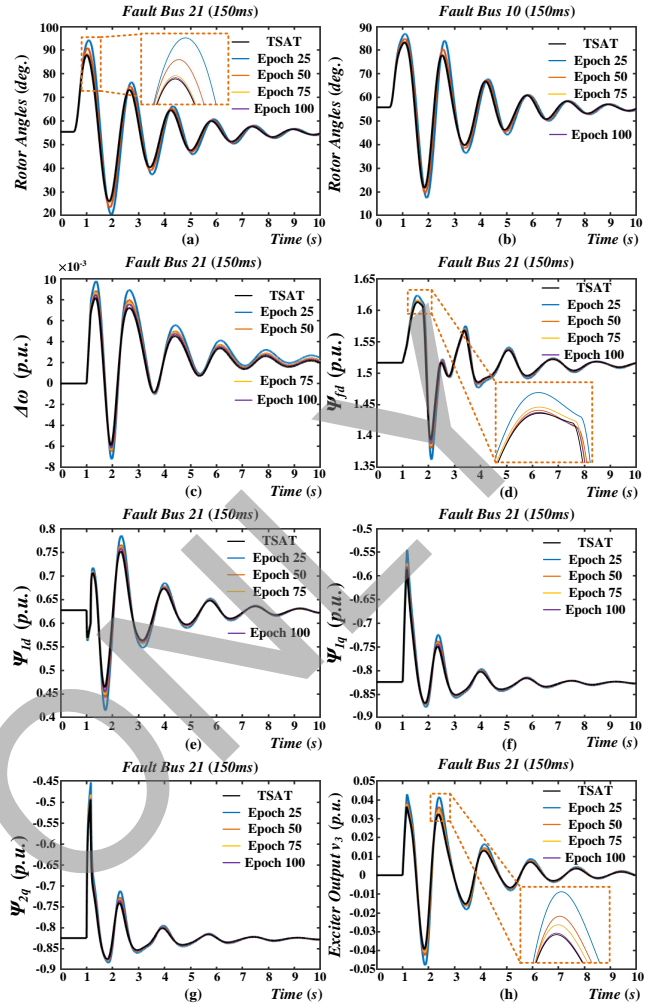


FIGURE 8. Outputs of Gen 10 under various epoch numbers: (a) rotor angles of a 150 ms fault at Bus 21, (b) rotor angles of a 150 ms fault at Bus 10, and results of a 150 ms fault at Bus 21: (c)  $\Delta\omega_1$ , (d)  $\psi_{fd}$ , (e)  $\psi_{1d}$ , (f)  $\psi_{1q}$ , (g)  $\psi_{2q}$ , and (h)  $v_3$ .



FIGURE 9. Representation of three-phase-to-ground fault in power system stability studies.

accuracy can be obtained. In order to test the generalization ability, the proposed SGM is also applied on other power transmission systems under various evaluation conditions that differ from the training datasets, as given in Table 2. As for IEEE 39-bus system 200 ms three-phase-to-ground faults are tested under various epoch numbers on the remaining 9 buses that are not included in the training dataset. In IEEE 118-bus system and 500-bus system, 250 ms and 270 ms three-phase-to-ground faults are tested under various epoch numbers on 10 buses that are not considered in the training dataset, respectively. The relative errors given in Table 2

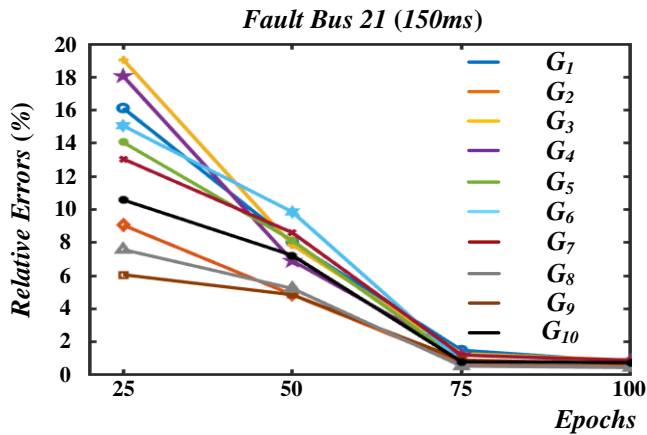


FIGURE 10. Relative errors of various training epochs.

TABLE 3. Hardware resource occupation of various methods

Module	Latency	BRAM	DSP	FF	LUT
NR	1526 $T_{clk}$	18	1296	287589	338067
RK4	199 $T_{clk}$	16	315	29709	45721
GRU-SGM	146 $T_{clk}$	42	116	13058	17064
Network	269 $T_{clk}$	16	534	43928	57664
XCVU9P	–	4320	6840	2364480	1182240

are the maximum relative errors among the 17 GRU-SGM output variables of the 9 or 10 three-phase faults in each system. Although the epoch number, and the subsequent networks would influence the accuracy of the trained model, the relative errors of GRU-SGM in various power systems are less than 1% after 100 epoch. And a minimum error of 0.65% can be obtained on the IEEE 39-bus system. Therefore, the accuracy can be guaranteed by the GRU method for dynamic security analysis.

Meanwhile, the GRU-based synchronous generator models and computational models are also executed on the Xilinx Virtex® UltraScale+™ VCU118 board containing XCVU9P FPGA to validated the efficiency. For the computational model, both the implicit Newton-Raphson (NR) method and explicit 4<sup>th</sup>-order Runge-Kutta (RK4) method are adopted for calculating the 17<sup>th</sup>-order DAEs. The hardware resource utilization and the latencies of various calculation strategies are provided in Table 3. The proposed GRU-SGM has significant advantages in resource consumption and execution time compared with NR method and RK4. Under the FPGA frequency of 100 MHz, the latency is defined in clock cycles which is 10 ns. Therefore, an FTRT ratio of  $\frac{1ms}{146 \times 10ns} = 684$  can be reached by applying the GRU-SGM.

### III. PART II: MACHINE LEARNING BASED DYNAMIC EQUIVALENCING FOR HYBRID AC-DC GRID

With the system scale becoming larger, despite the availability of high-performance hardware, the most time-consuming part of TS simulation is still solving the nonlinear DAEs of the synchronous generator. The dynamic equivalencing is therefore proposed to reduce the execution time, which

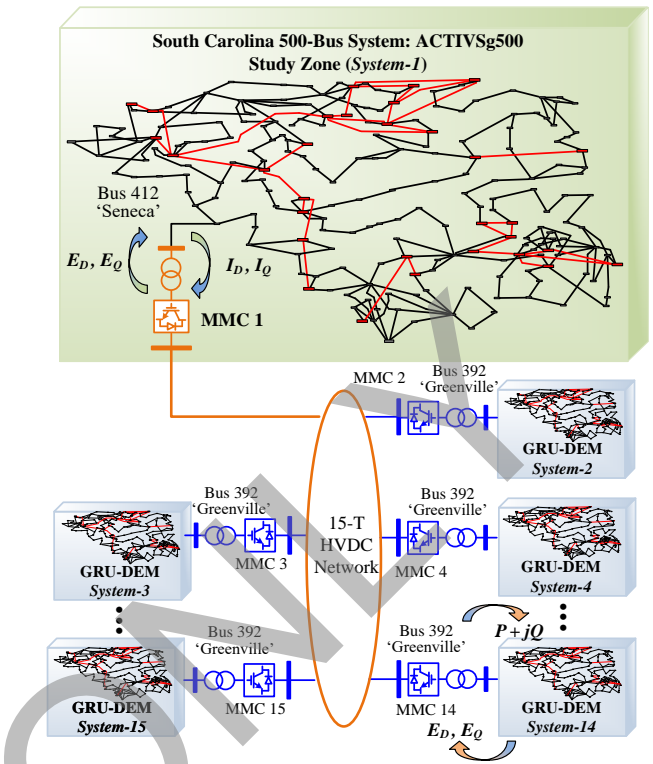


FIGURE 11. Hybrid computational-ML based test system of large-scale AC-DC grid.

is achieved by reducing the number of generator and the network nodes. The basic idea of dynamic equivalents for TS simulation is through the dynamic respond measurements to create an equivalent system that replaces a part of original system, where the equivalent models can be linear or non-linear. In this section, an GRU-based dynamic equivalents is proposed, which replaces the conventional procedures of dynamic equivalencing.

The external system refers to a nonlinear dynamic system with generators, excitors, and loads, which is replaced by the dynamic equivalent model (DEM) using machine learning techniques. The internal system represents the area that need to be analyzed in details, which is also called as study zone. The key issues of the proposed GRU-based dynamic equivalents are the quality of selected input/output signals, and the interface strategy between external area and study zone.

#### A. DATASETS AND TRAINING

The proposed GRU-based dynamic equivalent model is applied to a hybrid AC-DC grid, which contains fifteen ACTIVSg 500-bus systems and a fifteen terminal (15-T) HVDC grid, as given in Fig. 11 (a). The modular multilevel converter (MMC) 1 is treated as rectifier station, which provides the dynamic power to the 15-T HVDC grid and the external systems. The 500-bus System-1 is defined as the study zone, while the remaining fourteen 500-bus systems are replaced

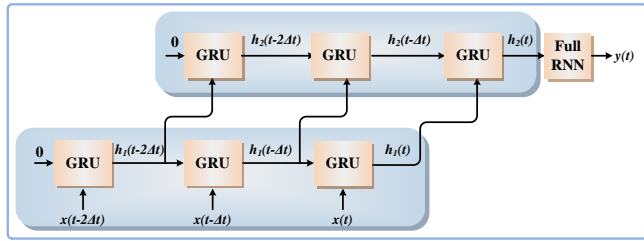


FIGURE 12. GRU structure for dynamic equivalent model of the external system.

by the GRU-based dynamic equivalent model, as shown in Fig. 11. Meanwhile, the GRU-SGM is also applied to *System-1* to represent the synchronous generators. As the 500-bus system contains 90 generators, the training time for synchronous generators will be extremely long. In order to reduce the training time, the 90 generators are divided into 5 groups depending on the output power, e.g., 0-200 MW, 200-400 MW, ..., and 800-1000 MW. The generators in each group share the same control system and mechanical system parameters. Therefore, only 5 GRU-SGMs need to be trained in a 500-bus system, and the differences among the generators in each group are the mechanical torques. After a disturbance in study zone, the output current at *Bus 412* starts to oscillate, and the oscillation will spread to the following external systems through the HVDC grid. Fig. 11 illustrates that the inverter stations provide dynamic  $P+jQ$  loads to the external systems at the boundary buses. In return, the external systems modeled by GRU-DEM provide the point of common coupling (PCC) voltages to the DC grid in the same manner.

Due to the relatively small size of the measurement values at the boundary buses between the DC grid and DEM, the datasets have significant impacts on the accuracy of the equivalent results, and therefore, a large number of contingencies in the study zone need to be included. In this work, the three-phase-to-ground faults occur at 90 buses are simulated off-line to obtain the real and imaginary components of the boundary nodes power and voltages. Meanwhile, for those contingencies that are cleared around the critical clearing time (CCT), the simulation result is highly sensitive to the error. The fault durations ranging from 50 ms-240 ms are simulated for training GRU to guarantee the accuracy of the proposed dynamic equivalent model, which means there are 20 various fault durations are simulated on each bus with a step of 10 ms. Therefore, the results of 1800 contingencies are collected from the off-line simulation tool for training the GRU-DEM. Due to the complexity of the 500-bus system, the maximum offline simulation time of a three-phase-to-ground fault is 27 s, which means about 14 h is needed for obtaining the training dataset. This time can be significantly reduced by considering the off-line simulation on a CPU cluster.

Although the structure of GRU-DEM is similar to that of the GRU-SGM, the hyper-parameters (hidden size, the number of layers, etc.) are different. The GRU structure for

TABLE 4. Relative errors of GRU-DEM

Output Variables	25 Epoch	50 Epoch	75 Epoch	100 Epoch
$E_D$	14.06%	8.13%	1.21%	0.78%
$E_Q$	13.13%	9.85%	2.81%	0.70%

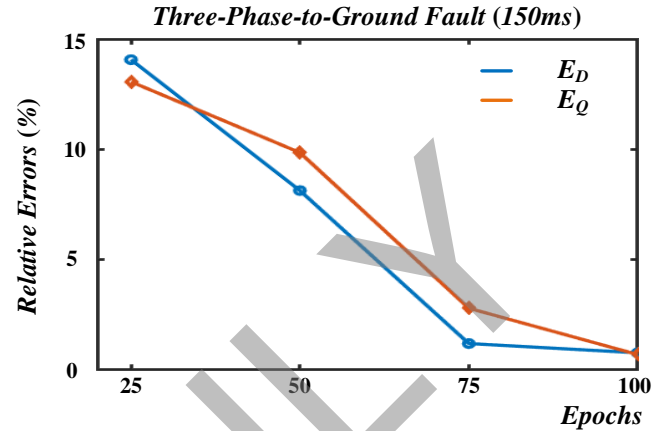


FIGURE 13. Relative errors of GRU-DEM under various training epochs.

DEM is illustrated in Fig. 12, where the input vector  $\mathbf{X}$  for GRU-DEM can be defined as:

$$\mathbf{X} = [P(t), Q(t), P(t-\Delta t), Q(t-\Delta t), P(t-2\Delta t), Q(t-2\Delta t)]^T. \quad (31)$$

Due to the complexity of the 500-bus system and the relatively small size of input data, the GRU-based model for DEM should increase much more hidden neurons (100 for DEM system), and the number of layers is two instead. With this comes increased data requirements. Nevertheless, the chosen auto-learning-rate optimization method, Adam algorithm [25], still works for this GRU-based model, and the training process costs about 30 h in one cluster node. Since the 500-bus systems have the same topology and control parameters, once one GRU-DEM system is trained and tested, other GRU-DEM systems can be trained and tested with their own datasets in the same GRU model to shrink the training time. Meanwhile, taking the data collection time into consideration, the total time for training the GRU-SGM is about  $14 + 30 = 44h$ . In order to further demonstrate the relationship between epoch numbers and model accuracy, the relative errors under various epochs are illustrated in Fig. 13 after a three-phase-to-ground fault lasting 150 ms in the study zone. Meanwhile, 10 three-phase-to-ground faults lasting 270 ms are emulated in *System-1* under various epoch numbers. The maximum relative errors of output value  $E_d$  and  $E_q$  among the 10 faults are given in Table 4, which indicates that the accuracy of the proposed GRU-DEM can be guaranteed after 100 epochs.

### B. DC GRID MODELING

In order to reflect the dynamic process of the 15-T HVDC grid, the electromagnetic transient (EMT) simulation with a time-step of 200  $\mu s$  is adopted. Since the less hardware



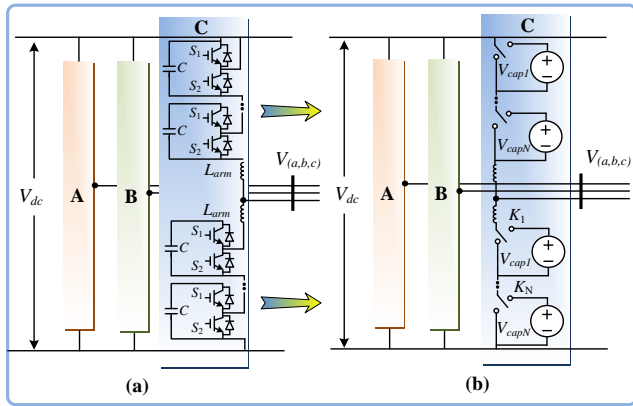


FIGURE 14. Illustration of modular multilevel converter modeling: (a) three-phase topology, (b) average value model.

resource is preferred for hardware design, the average value model (AVM) is applied to emulate MMC stations to obtain a higher FTRT ratio. The configuration of a three-phase MMC interconnecting with AC and DC grid is given in Fig. 14 (a), which contains  $N$  half-bridge submodules (HBSMs) and an arm inductor on each arm. A brief introduction of MMC AVM is presented here, further information can be found in [26]- [27]. Each HBSM can be modeled as a controlled voltage source to simplify the calculation as shown in Fig. 14 (b). Assuming that the capacitor voltages are well balanced, which means the average values of capacitor voltages are equal. The equivalent voltage source of an arbitrary submodule can be expressed as

$$V_{ave} = V_{cap1} = \dots = V_{capN} = \frac{V_{dc}}{N}, \quad (32)$$

$$V_{SMi} = K(i) \cdot \frac{V_{dc}}{N}, \quad (33)$$

where  $K(i)$  refers to the switching function that takes the value 1 when the submodule capacitor is inserted and 0 when the submodule is bypassed. Then the output voltage on each arm can be derived as

$$V_{arm} = \sum_{i=1}^N K(i) \cdot \frac{V_{dc}}{N} + L_{arm} \frac{dI_{arm}}{dt}, \quad (34)$$

The well-balanced condition in the AVM yields no circulating current, resulting in the differential term in (34) can be neglected. The output voltage on each phase can be calculated as

$$V_{a,b,c} = \sum_{i=1}^N (K_u(i) - K_l(i)) \cdot \frac{V_{dc}}{N} + L_{arm} \frac{dI_{arm}}{dt}, \quad (35)$$

where  $K_u(i)$  and  $K_l(i)$  represent the upper and lower arms switching functions, respectively.

Since the EMT simulation is adopted in the DC system, the reactive components such as the capacitor and inductor are expressed by ordinary differential equations, which should be discretized before numerical calculating. Trapezoidal rule

is utilized for this purpose in HVDC grid so that a discrete-time Norton equivalent circuit is generated. The impedances of the capacitor and inductor and the corresponding current sources of the Norton equivalent circuit are given as:

$$Z_{Ceq} = \frac{\Delta t}{2C}, \quad (36)$$

$$I_{Ceq}(t) = -I_C(t - \Delta t) - \frac{2C}{\Delta t} \cdot V_C(t - \Delta t), \quad (37)$$

$$Z_{Leq} = \frac{2L}{\Delta t}, \quad (38)$$

$$I_{Leq}(t) = I_L(t - \Delta t) + \frac{\Delta t}{2L} \cdot V_L(t - \Delta t). \quad (39)$$

Due to the adoption of the small time-step, the one-step integration method is able to guarantee the accuracy of EMT simulation, which also reduces the computational burden compared with higher order integration methods.

### C. INTERFACE STRATEGY OF HYBRID COMPUTATIONAL-ML BASED DYNAMIC SYSTEM EQUIVALENCING

Since the DC grid undergoes the EMT simulation and the TS simulation is applied on the 500-bus *System-1* in the study zone, it would be impractical to take the two types of simulation model running compatible instantly. Meanwhile, the generators of *System-1* applies the GRU-SGM while the remaining 500-bus systems are represented by the GRU-DEM. An interface strategy should be designed properly at the boundary buses. As illustrated in Fig. 11, the DC grid provide PCC voltage in  $D$ - $Q$  frame to the AC system, while the TS simulation part provide current to the rectifier station. Therefore, from the AC system point of view, the DC grid can be simplified as a dynamic voltage source interconnecting with the network equations. The DC grid provide the PCC voltage to the network, resulting in the non-zero value at the boundary bus. And (27) can be further expanded as

$$\begin{bmatrix} \mathbf{I}_i^{ML} \\ \mathbf{I}_b^{DC} \end{bmatrix} = \begin{bmatrix} \mathbf{Y}_{ii} & \mathbf{Y}_{ib} \\ \mathbf{Y}_{bi} & \mathbf{Y}_{bb} \end{bmatrix} \begin{bmatrix} \mathbf{E}_i^{ML} \\ \mathbf{E}_b^{DC} \end{bmatrix}, \quad (40)$$

where the subscript  $i$  is the generator nodes that are represented by the ML-based SGM, the superscript  $DC$  represents the variables coming from DC grid, and  $b$  refers to the boundary node of AC and DC grids which is *Bus 412* in the study zone. As the PCC voltage calculated by the HVDC grid in  $D$ - and  $Q$ - axis are already known, the current injection at the boundary bus can be derived as a complex matrix equations.

$$\mathbf{I}_b^{DC} = \mathbf{Y}_{bi} \mathbf{E}_i^{ML} + \mathbf{Y}_{bb} \mathbf{E}_b^{DC}. \quad (41)$$

As mentioned, the generator voltages  $\mathbf{E}_i^{ML}$  are not directly known after solving the GRU-DEM, the relationship between generator voltages and currents can be expressed in (28) and (29). Obviously, the only unknown vector in (40) is  $\mathbf{I}_b^{DC}$ , and therefore, the output current at the boundary bus can be solved and is sent to DC grid to keep the EMT emulation going on. The hardware emulation procedure of the AC-DC grid digital twin is similar to that of the IEEE 39-bus system as given in Fig. 7, where the *Step 2* is replaced by solving the MMC AVM and GRU-DEM/SGM.



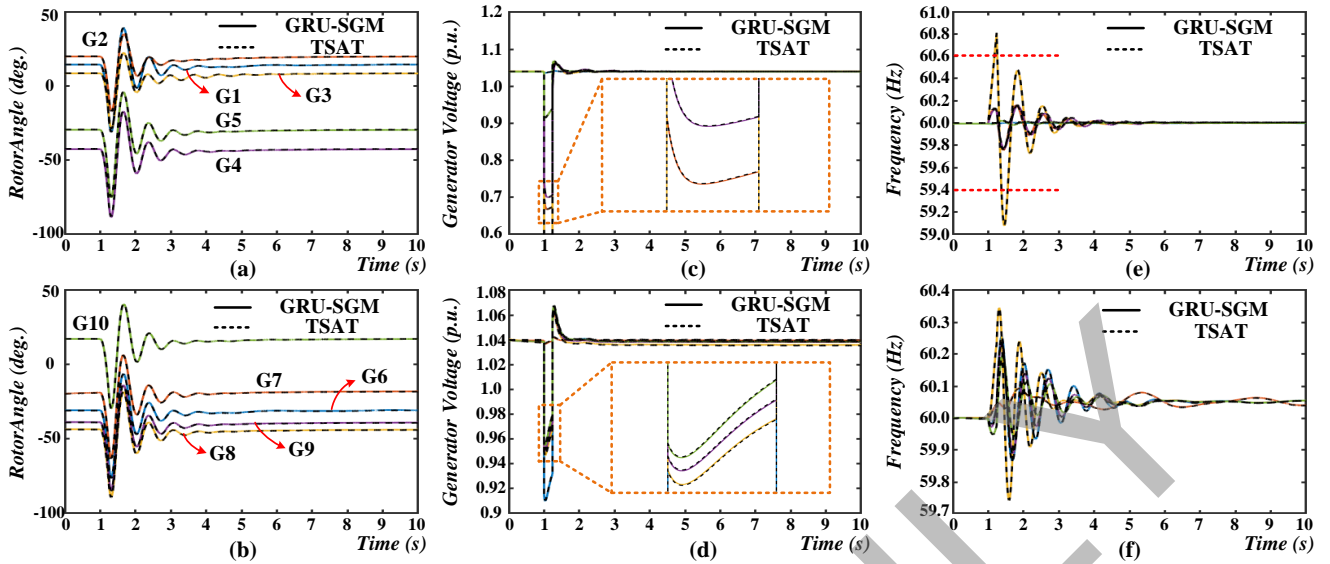


**FIGURE 16.** Comparison of GRU-SGM and TSAT<sup>®</sup> results under three-phase-to-ground fault: (a) generator rotor angles (G1-G5), (b) generator rotor angles (G6-G10), (c) generator output voltages (G1-G5), (d) generator output voltages (G6-G10), (e) generator frequencies (G1-G5), and (f) generator frequencies (G6-G10).

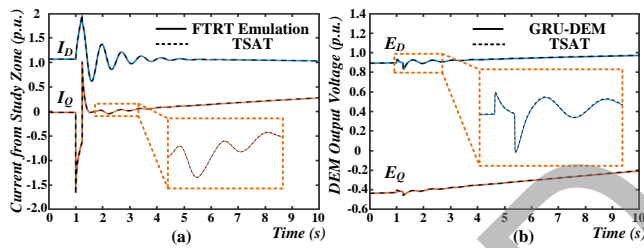


**FIGURE 17.** FTERT emulation results of interface data: (a) output currents at Bus 412 of study zone, (b) output voltages of GRU-DEM.

## V. HARDWARE EMULATION RESULTS AND VALIDATION

The hardware emulation of the integrated AC-DC grid was conducted on the FPGA-based FTERT digital twin platform as mentioned above, and the emulation results of the proposed GRU-based synchronous generator and dynamic equivalent model were validated by comparing with the results from the off-line simulation tool DSATools<sup>TM</sup>/TSAT<sup>®</sup>.

### A. CASE 1: THREE-PHASE-TO-GROUND FAULT

In dynamic security analysis, the three-phase-to-ground faults usually induce the most severe disturbances. Meanwhile, the emulation results for those contingencies that are cleared around the CCT are usually highly sensitive to the error, and therefore, a three-phase-to-ground fault on the study zone lasting 300 ms is taken into considered in this part. Under steady-state, the study zone delivers 850 MW to the remaining 500-bus systems via the 15-T HVDC grid, and each system receives about 50 MW. At the time of 1 s, a three-phase fault takes place at Bus 413 with a duration of 300 ms. Since the fault location is close to the PCC Bus 412, the fault will cause serious oscillation and spread to the

following systems. The emulation results of G1 to G10 are provided in Fig. 16. When the fault encounters, the generator rotor angles experience a drastic oscillation lasting about 3 s. A significant voltage drop occurs right after the occurrence the three-phase fault as given in Fig. 16 (c) and (d). In the meantime, the abnormal rotor angles induce a severe oscillation on the generator frequencies, and the frequency of G3 exceed the  $\pm 1\%$  threshold as shown in Fig. 16 (e) and (f).

To validate the accuracy of the proposed GRU-DEM, the interface data is also provided in Fig. 17. The oscillating currents in  $D$ - $Q$  frame at Bus 412 are send to the rectifier station and delivered to the subsystems that are emulated by DEM. Due to the 14 subsystems connected to the HVDC grid, the output voltage of each DEM system is not as severe as the output current from the study zone as shown in Fig. 17 (b). The zoomed-in plots in Fig. 17 and Fig. 16 (c)-(d) indicate that the FTERT emulation results match up with that of the TSAT<sup>®</sup>, which proves that the proposed GRU-SGM and DEM is as accurate as the transient stability simulation of the full system in TSAT<sup>®</sup>.

### B. CASE 2: GENERATION REDUCTION

The proposed dynamic equivalent model was trained by several three-phase faults, and the accuracy can be guaranteed as mentioned above. In the dynamic security analysis, the system may encounter several kinds of contingencies. In this section, a long-term generation reduction is emulated on the FTERT platform and validated by the off-line simulation tool. The generation reduction disturbance is emulated by reducing the mechanical torque of the GRU-SGM. As given in Fig. 1, the synchronous generator is driven by five steam-turbine. According to (4)-(9), the mechanical torque can be



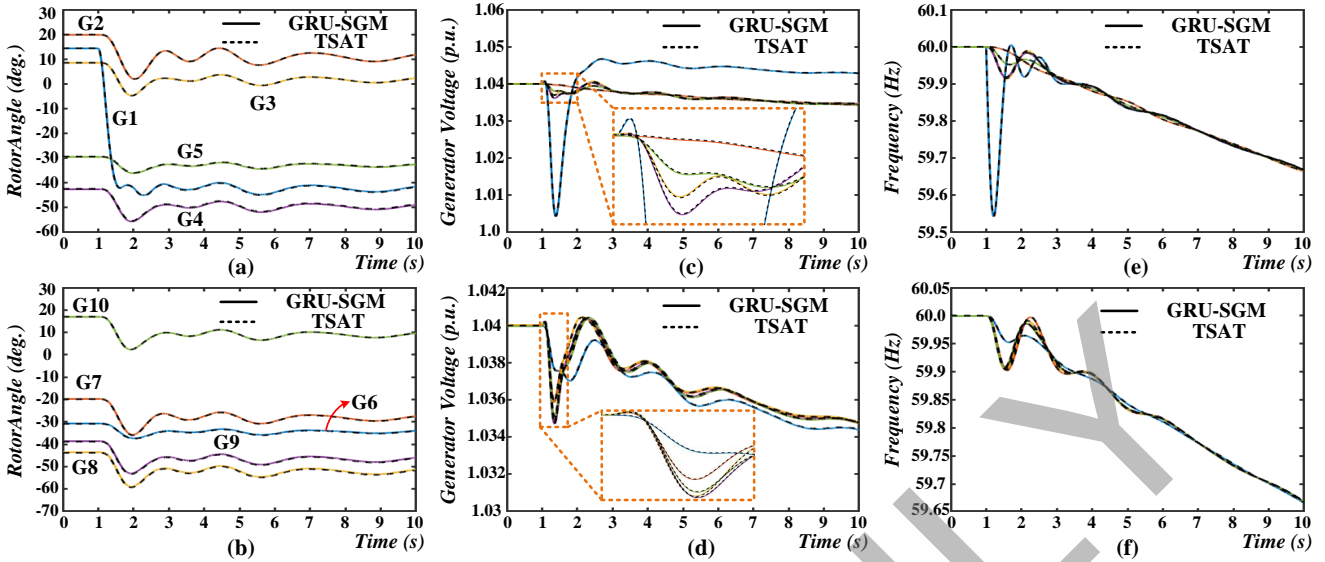


**FIGURE 18.** Comparison of GRU-SGM and TSAT<sup>®</sup> results under generation reduction on G1: (a) generator rotor angles (G1-G5), (b) generator rotor angles (G6-G10), (c) generator output voltages (G1-G5), (d) generator output voltages (G6-G10), (e) generator frequencies (G1-G5), and (f) generator frequencies (G6-G10).

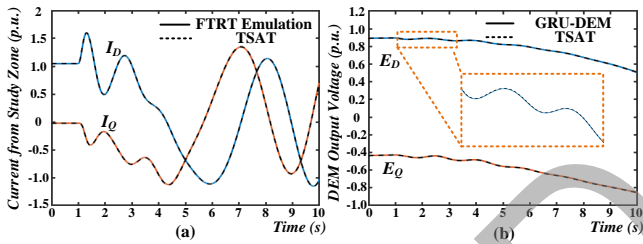


**FIGURE 19.** FTRT emulation results of interface data: (a) output currents at Bus 412 of study zone, (b) output voltages of GRU-DEM.

expressed as:

$$T_m(t) = T_1(t) + T_2(t) + T_3(t) + T_4(t) + T_5(t). \quad (42)$$

At the time of 1 s, the mechanical torque in G1 suddenly reduce 90% of its normal operation without recovered. Since  $T_{1-5}(t)$  are the inputs of GRU-SGM, changing the mechanical torque will not affect the performance of the proposed model. The imminent impacts including serious disturbance to the rotor angles, generator voltages, and frequencies, as given in Fig. 18. The frequencies of synchronous generators keep decreasing and cannot be restored. Due to the  $\pm 1\%$  threshold of the frequencies in dynamic security assessment, the abnormal frequencies are detected after 10 s, which may cause serious impacts on the system. With the 208 FTRT ratio, the hardware emulation platform is able to predict the upcoming disturbance and take remedial actions.

Similarly, the interface data is also provided to validate the accuracy of the proposed DEM under generation reduction, as given in Fig. 19. Fig. 19 (a) indicates that the reduced generation causes output current at Bus 412 unstable. The zoomed-in plots in Fig. 19 (b) proves that the proposed DEM still has high accuracy under the contingencies except three-

phase faults. Therefore, the proposed GRU-SGM and DEM executed on the FTRT emulation platform can be utilized on large-scale AC-DC grid for dynamic security analysis.

### C. CASE 3: LOAD CHANGE

To further demonstrate the accuracy of the proposed GRU-DEM and GRU-SGM, a sudden load change fault is also tested, as given in Fig. 20. The load change disturbance is emulated by changing the  $P_{Load}$  and  $Q_{Load}$  values in (25). At 1 s, a load of 400 MW is suddenly removed in the study zone, causing the instability to the AC system which cannot be recovered. As can be seen in Fig. 20 (e) and (f), the frequencies keep rising and eventually they are far beyond the maximum allowed 1 % threshold. The dashed lines refer to the results from the off-line simulation tool TSAT<sup>®</sup>, while the solid lines represent the results from the proposed GRU-SGM. The zoomed-in figures in Fig. 20 (e) and (f) prove that the GRU-SGM is still accurate during the severe load change fault.

Meanwhile, in such an integrated network, the disturbances after sudden load change also spread to the following 14 subsystems through the 15-T HVDC grid. Fig. 21 (a) shows that the sudden load change causes severe oscillation at the boundary bus. Since the responses of the fourteen subsystems modeled in GRU-DEM are similar after the load change, only the output voltages of System 2 are provided in Fig. 21 (b). It indicates that the output voltages calculated from the proposed GRU-DEM are matched with the results from TSAT<sup>®</sup>. As mentioned, the acceleration of digital twin hardware emulation is more than 208 times faster than real-time, which means the proposed FTRT emulation equipped in the energy control center has sufficient time to deal with dynamic security assessment to initiate proper control actions.



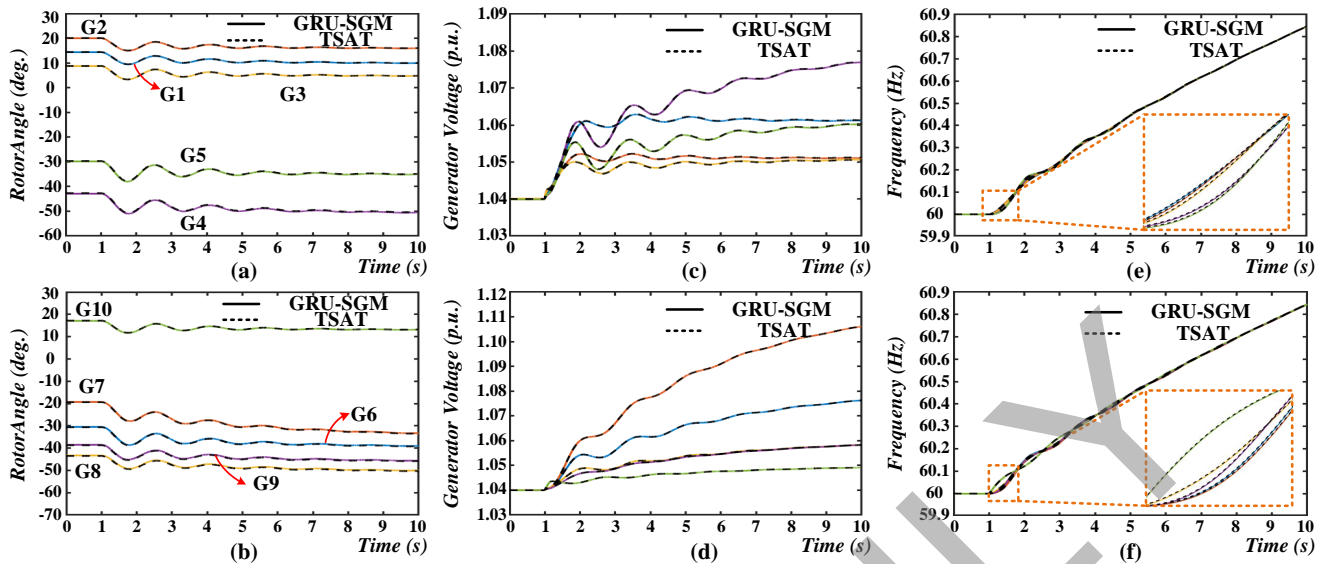


**FIGURE 20.** Comparison of GRU-SGM and TSAT<sup>®</sup> results under sudden load change fault in study zone: (a) generator rotor angles (G1-G5), (b) generator rotor angles (G6-G10), (c) generator output voltages (G1-G5), (d) generator output voltages (G6-G10), (e) generator frequencies (G1-G5), and (f) generator frequencies (G6-G10).

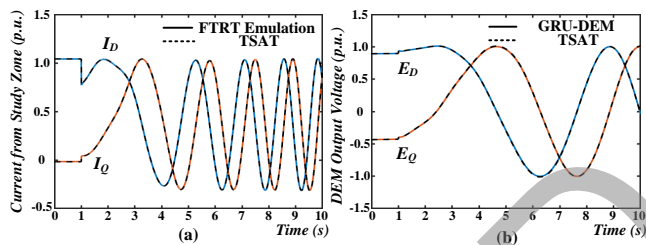


**FIGURE 21.** FTRT emulation results of interface data: (a) output currents at Bus 412 of study zone, (b) output voltages of GRU-DEM.

## VI. CONCLUSION

This paper proposed the ML based synchronous generator model and dynamic equivalent model for implementing an FTRT digital twin of a large-scale AC-DC grid. The GRU-based ML strategy is able to emulate the multi-mass synchronous machine with high accuracy. Compared with traditional iterative method, the GRU-based machine model has significant advantages in resource consumption and execution time during hardware implementation. Meanwhile, the GRU-based ML method is also applied to create a dynamic equivalent system. Since the GRU-DEM replaces the complex computational model in the external system, the execution time of emulating the hybrid AC-DC grid is accelerated. The utilization of the FPGA boards containing the high-speed communication interfaces enabled emulating a large-scale power system in parallel, and a 208 FTRT ratio was achieved. Furthermore, two case studies were emulated to validate the accuracy of the proposed model with contingencies that differ from the training datasets. The FTRT hardware emulation results of the integrated AC-DC grid are highly matched with those of the off-line simulation results from TSAT<sup>®</sup>. Therefore, the GRU-SGM and DEM executed on the FPGA-

based FTRT emulation platform can help predict upcoming disturbances and initiate remedial actions, which is significantly meaningful in an energy control center application.

## REFERENCES

- [1] M. L. Ourari, L. -A. Dessaint, and V. -Q Do, "Dynamic equivalent modeling of large power systems using structure preservation technique," *IEEE Trans. Power Syst.*, vol. 21, no. 3, pp. 1284-1295, Aug. 2006.
- [2] U. D. Annakkage, N. K. C. Nair, Y. Liang, A. M. Gole, V. Dinavahi, B. Gustavsen, T. Noda, H. Ghasemi, A. Monti, M. Matar, R. Iravani, and J. A. Martinez, "Dynamic system equivalents: a survey of available techniques," *IEEE Trans. Power Del.*, vol. 27, no. 1, pp. 411-420, Jan. 2012.
- [3] R. J. Galarza, J. H. Chow, W. W. Price, A. W. Hargrave, and P. M. Hirsch, "Aggregation of exciter models for constructing power system dynamic equivalents," *IEEE Trans. Power Syst.*, vol. 13, no. 3, pp. 782-788, Aug. 1998.
- [4] Y. Zhou, L. Zhao, and W. -J. Lee, "Robustness analysis of dynamic equivalent model of DFIG wind farm for stability study," *IEEE Trans. Ind. App.*, vol. 54, no. 6, pp. 5682-5690, Nov. 2018.
- [5] I. Tyuryukanov, M. Popov, M. A. M. van der Meijden, and V. Terzija, "Slow coherency identification and power system dynamic model reduction by using orthogonal structure of electromechanical eigenvectors," *IEEE Trans. Power Syst.*, vol. 36, no. 2, pp. 1482-1492, Mar. 2021.
- [6] I. J. Perez-arriaga, G. C. Verghese, and F. C. Schweppes, "Selective modal analysis with application to electric power systems, part I: heuristic introduction," *IEEE Trans. Power App. Syst.*, vol. PAS-101, no. 9, pp. 3117-3125, Sep. 1982.
- [7] I. J. Perez-arriaga, G. C. Verghese, and F. C. Schweppes, "Selective modal analysis with application to electric power systems, part II: the dynamic stability problem," *IEEE Trans. Power App. Syst.*, vol. PAS-101, no. 9, pp. 3126-3134, Sep. 1982.
- [8] G. Troullos, J. F. Dorsey, H. Wong, J. Myers, and S. Goodwin, "Estimating order reduction for dynamic equivalents," *IEEE Trans. Power App. Syst.*, vol. PAS-104, no. 12, pp. 3475-3481, Dec. 1985.
- [9] Y.-N. Yu, and M. A. El-Sharkawi, "Estimation of external dynamic equivalents of a thirteen-machine system," *IEEE Trans. Power App. Syst.*, vol. PAS-100, no. 3, pp. 1324-1332, Mar. 1981.
- [10] P. Ju, L. Q. Ni, and F. Wu, "Dynamic equivalents of power systems with online measurements. Part 1: theory," *Proc. Inst. Elect. Eng. Gen. Transm. Distrib.*, vol. 151, no. 2, pp. 175-178, Mar. 2004.
- [11] P. Ju, L. Q. Ni, and F. Wu, "Dynamic equivalents of power systems with online measurements. Part 2: applications," *Proc. Inst. Elect. Eng. Gen. Transm. Distrib.*, vol. 151, no. 2, pp. 179-182, Mar. 2004.

[12] A. T. Sarič, M. T. Transtrum, and A. M. Stankovič, "Data-driven dynamic equivalents for power system areas from boundary measurements," *IEEE Trans. Power Syst.*, vol. 34, no. 1, pp. 360-370, Jan. 2019.

[13] G. A. Barzegkar-Ntovom, T. A. Papadopoulos, and E. O. Kontis, "Robust framework for online parameter estimation of dynamic equivalent models using measurements," *IEEE Trans. Power Syst.*, vol. 36, no. 3, pp. 2380-2389, May 2021.

[14] J. H. Chow, *Power System Coherency and Model Reduction*, Springer New York, 2013.

[15] Q. Liu, T. Liang, and V. Dinavahi, "Real-time hierarchical neural network based fault detection and isolation for high-speed railway system under hybrid AC/DC grid," *IEEE Trans. Power Del.*, vol. 35, no. 6, pp. 2853-2864, Dec. 2020.

[16] V. Dinavahi, and N. Lin, *Real-Time Electromagnetic Transient Simulation of AC-DC Networks*, Wiley-IEEE Press, 2021.

[17] P. Kundur, *Power System Stability and Control*, New York: McGraw-Hill, 1994.

[18] D. F. Specht, "A general regression neural network," *IEEE Trans. Neural Netw.*, vol. 5, no. 2, pp. 157-166, Mar. 1994.

[19] K. Y. Lee, Y. T. Cha, and J. H. Park, "Short-term load forecasting using an artificial neural network," *IEEE Trans. Power Syst.*, vol. 7, no. 1, pp. 124-132, Feb. 1992.

[20] M. Schuster and K. K. Paliwal, "Bidirectional recurrent neural networks," *IEEE Trans. Signal Process.*, vol. 45, no. 11, pp. 2673-2681, Nov. 1997.

[21] J. Chung, C. Gulcehre, K. Cho, and Y. Bengio, "Empirical evaluation of gated recurrent neural networks on sequence modeling," arXiv:1412.3555 [cs], Dec. 2014.

[22] S. Hochreiter and J. Schmidhuber, "Long short-term memory," *Neural Comput.*, vol. 9, no. 8, pp. 1735-1780, Nov. 1997.

[23] D. Zhang and M. R. Kabuka, "Combining weather condition data to predict traffic flow: A GRU-based deep learning approach," *IET Intell. Transp. Syst.*, vol. 12, no. 7, pp. 578-585, Sept. 2018.

[24] S. Zhang, T. Liang and V. Dinavahi, "Machine learning building blocks for real-time emulation of advanced transport power systems," *IEEE Open J. Power Electron.*, vol. 1, pp. 488-498, Nov. 2020.

[25] D. P. Kingma, and J. Ba, "Adam: A method for stochastic optimization," arXiv:1412.6980 [cs], Dec. 2014.

[26] H. Yang, Y. Dong, W. Li, and X. He, "Average-value model of modular multilevel converters considering capacitor voltage ripple," *IEEE Trans. Power Del.*, vol. 32, no. 2, pp. 723-732, Apr. 2017.

[27] A. Beddard, C. E. Sheridan, M. Barnes, and T. C. Green, "Improved accuracy average value models of modular multilevel converters," *IEEE Trans. Power Del.*, vol. 31, no. 5, pp. 2260-2269, Oct. 2016.



programmable gate arrays.

SHIQI CAO (S'19) received the B.Eng. degree in electrical engineering and automation from East China University of Science and Technology, Shanghai, China, in 2015, and the M.Eng. degree in power system from Western University, London, Ontario, Canada, in 2017. He is currently pursuing the Ph.D. degree in electrical and computer engineering with the University of Alberta, Canada. His research interests include transient stability analysis, power electronics, and field pro-



VENKATA DINAHAHI (S'94-M'00-SM'08-F'20) received the B.Eng. degree in electrical engineering from the Visveswaraya National Institute of Technology (VNIT), Nagpur, India, in 1993, the M.Tech. degree in electrical engineering from the Indian Institute of Technology (IIT) Kanpur, India, in 1996, and the Ph.D. degree in electrical and computer engineering from the University of Toronto, Ontario, Canada, in 2000. Presently he is a Professor with the Department of Electrical and Computer Engineering, University of Alberta, Edmonton, AB, Canada. He is a fellow of the Engineering Institute of Canada. His research interests include real-time simulation of power systems and power electronic systems, electromagnetic transients, devicelevel modeling, large-scale systems, and parallel and distributed computing.



NING LIN (S'17) received the B.Sc. and M.Sc. degrees in Electrical Engineering from Zhejiang University, China, in 2008 and 2011, respectively, and the Ph.D. degree in Electrical and Computer Engineering from the University of Alberta, Canada, in 2018. His research interests include power systems analysis and simulation, power electronics, and high-performance computing.

...